ESTIMATION OF 511 keV GAMMA SCATTER FRACTION IN WLS LAYER IN TOTAL-BODY J-PET; A SIMULATION STUDY*

K. Tayefi Ardebili, S. Niedzwiecki, P. Moskal

Faculty of Physics, Astronomy, and Applied Computer Science
Jagiellonian University
Łojasiewicza 11, 30-348 Kraków, Poland
and
Center for Theranostics, Kopernika 40, 31-034 Kraków, Poland
and
Total-Body Jagiellonian-PET Laboratory, Jagiellonian University
Łojasiewicza 11, 30-348 Kraków, Poland

Received 24 October 2022, accepted 14 November 2022, published online 28 November 2022

Positron emission tomography (PET) is essential in medical diagnostics and monitoring therapy. The J-PET Collaboration at Jagiellonian University is developing a new generation of Total-Body PET scanners based on plastic scintillators. One of the Total-Body J-PET designs comprises seven rings, each consisting of 24 modules. A single module is built of 2 layers, each comprises of 16 axially arranged plastic scintillator strips of 330 mm length, read out by silicon photomultiplier (SiPM) arrays from both ends, and an additional layer of 50 wavelength shifter (WLS) bars, placed perpendicular to plastic layers. This study estimates the scatter fraction of the Total-Body J-PET manufactured from plastic scintillator strips according to the NEMA NU 2-2018 standards by using the GATE software. The scatter phantom was simulated as a solid cylinder with a length of 700 mm and an outside diameter equal to 203 mm. At the same time, at a radial distance of 45 mm, we have a hole with a diameter of 6.4 mm where a linear source with total activity of 1 MBq is placed. For data processing, sinograms were generated, and the Single Slice Rebinning (SSRB) algorithm was used for the scatter fraction calculation. As a result, we estimate that addition of the WLS layer is increasing the scatter fraction by 0.67%.

DOI:10.5506/APhysPolBSupp.15.4-A7

* Presented at the 4th Jagiellonian Symposium on *Advances in Particle Physics and Medicine*, Cracow, Poland, 10–15 July, 2022.

1. Introduction

The Positron Emission Tomography (PET) scanners play a fundamental role in medical diagnostics and treatment monitoring [1]. A common PET system is based on the crystal scintillator, the annihilation photons are registered by the photoelectric effect. The photodetector is located behind the scintillator in the radial direction [2–11]. Most of the current clinically available PET scanners have a limited axial field of view (AFOV) around 15–26 cm [3, 12, 13]. Many groups try to improve the performance of PET scanners by increasing AFOV, *e.g.* the Jagiellonian Positron Emission Tomograph (J-PET) prototype [4, 14], Penn-PET [15–17], Explorer [18–20], and Quadra [21, 22]. The J-PET scanner is manufactured from plastic scintillator strips placed along the Z-axis, where the silicon photomultiplier (SiPM) is located at the end of the strips, and gamma detection is based on the Compton scattering [2, 23–29]. Currently, the J-PET Collaboration is developing a novel prototype of Total-Body scanner with an AFOV larger than 200 cm [14]. J-PET is a multi-photon (multi-gamma) scanner designed for the standard two-gamma PET imaging [14], as well as for three-photon [30] and positronium imaging [25, 29, 31–33].

In this article, we estimate the 511 keV gamma scatter fraction increase due to introduction of the WLS layer in Total-Body J-PET using the Geant4 Application for Tomography Emission (GATE) [34, 35]. The scatter fraction estimates the detector's sensitivity to scattered radiation [14, 15, 18]. It is one of the characteristics defined by the National Electrical Manufacturers Association (NEMA NU 2-2018) [36].

2. Method

2.1. Geometry

The considered design of the Total-Body J-PET scanner comprises 7 rings. As shown in Fig. 1, each ring is placed axially next to the other with a 20 mm gap. Each ring consists of 24 modules with a length of 330 mm and the inner diameter equal to 830 mm. Each module is built out of 3 layers [14]: the first and third layers consist of 16 plastic scintillator strips with dimensions of 6 mm × 30 mm × 330 mm placed next to each other, while the second layer is composed of wavelength shifter bars (WLS). The WLS layer is registering optical photons produced from the interaction of gamma with the plastic scintillator [37, 38]. The WLS layer can be utilized to improve the axial resolution and consists of the 50 WLS bars with dimensions of 3 mm × 6 mm × 108.15 mm (see Fig. 1 (D)), which are placed between the aforementioned two layers and are oriented perpendicularly to the plastic scintillators [37].

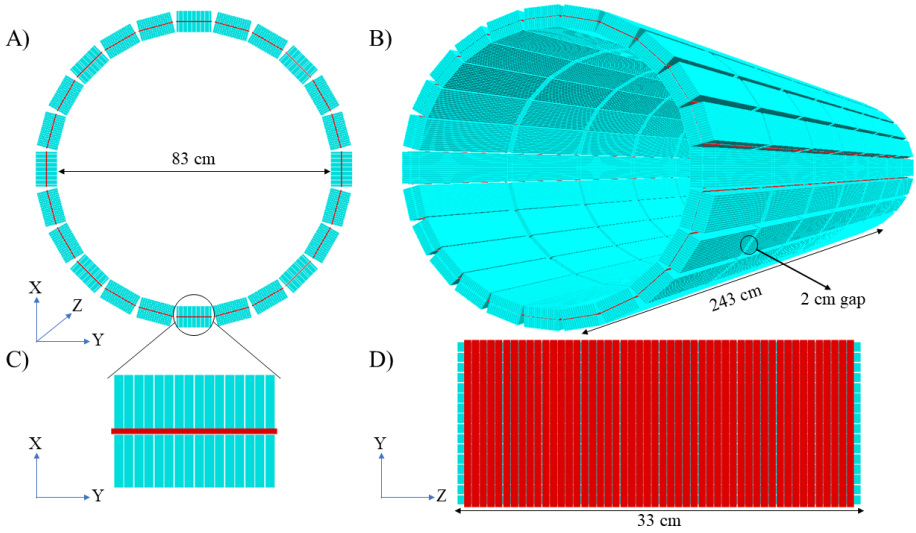

Fig. 1. Schematic view of simulated Total-Body J-PET. (A) The front view of the scanner, with the 830 mm inner diameter detection ring consisting of 24 modules. (B) The scanner consists of 7 detection rings with a length of 330 mm and a 20 mm gap between the rings for a total AFOV of 2430 mm. (C) Each module consists of 2 layers with a total of 32 strips of plastic scintillators (6 mm × 30 mm × 330 mm) with a thickness of 30 mm and width equal to 6 mm (shown with blue strips in the picture), and additional 50 bar strips (3 mm × 6 mm × 108.15 mm) called WLS (shown with the red strips in the picture). (D) The orientation of the WLS strips inside the module.

2.2. Simulation tools

In this study, simulations were performed by using the GATE [34, 35] version 9 based on the Geant4 version 4.10.06 with the digitizer "simulation toolkit", the analysis process is based on the coincidences part of the digitizer output. The energy window larger than 200 keV (see Fig. 2) in the fixed time window of 3 ns was selected [24]. Two simulations have been performed to evaluate the WLS layer's effect in the Total-Body J-PET configuration. The first simulation concerned Total-Body J-PET with the presence of a WLS layer, and the second one was performed without it.

2.3. Scatter fraction

The scatter fraction is one of the essential parameters according to the NEMA NU 2-2018 [2, 36]. The PET scanner scatter fraction estimates the detector's sensitivity to scattered radiation [14, 15, 18]. It is expressed as a ratio between the scattered coincidences and the sum of scattered and true coincidences [14, 15, 18, 39]. According to the NEMA standard, scat-

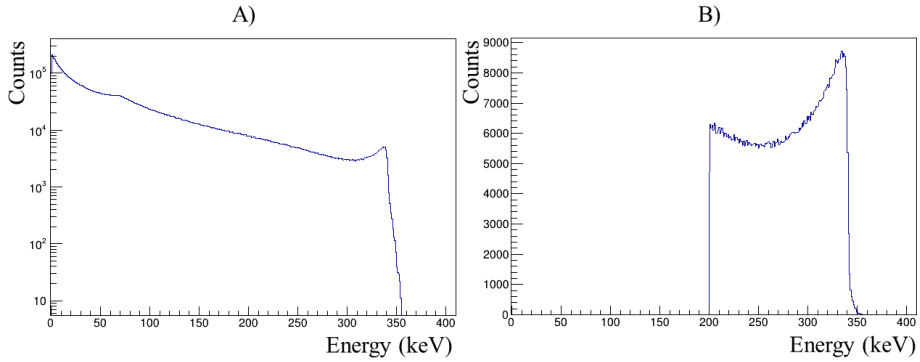

Fig. 2. Energy distribution of the gamma photons registered in coincidences. (A) Energy distribution before applying energy cuts in logarithmic scale. (B) Energy distribution after applying the energy cuts in the fixed time window.

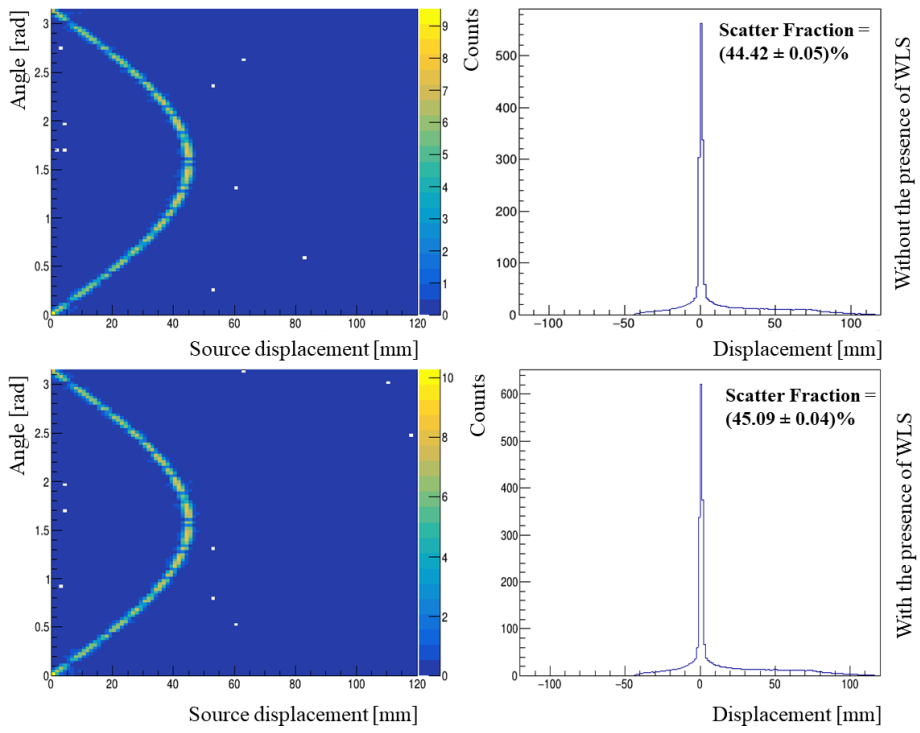

Fig. 3. Top: Simulations result for the Total-Body J-PET scanner without the WLS layer. Bottom: Simulations result for the Total-Body J-PET scanner with the WLS layer; with the 70 cm long source and 1 MBq total activity. Left: Sinogram for a whole scanner (vertical palette shows the counts). Right: Aligned to zero and summed sinogram.

ter fractions should be calculated by using SSRB algorithm. The SSRB algorithm is based on the divided space inside the scanner into N virtual slices and N^2 oblique sinograms [2]. They are generated for the variation of the line of response (LOR). One can use the SSRB algorithm to obtain $2N-1$ rebinned sinograms [2, 40]. In the next step rebinned sinograms are summed into one sinogram (see left panel of Fig. 3), and all projections are aligned in zero and summed with a maximum amount of counts to obtain a one-dimensional profile (see right panel of Fig. 3). The area below the line crossing two points at ±20 mm demonstrates the scatter coincidences and over that line, true coincidences [2].

To calculate the scatter fraction, a scatter phantom was simulated. NEMA NU 2-2018 requires a phantom with a 700 mm length for scanners with AFOV smaller than 65 cm [36] and for longer AFOV, a phantom of the same or longer length [18]. The simulated phantom is a solid cylinder composed of polyethylene [2, 14, 15, 18] with a specific gravity of 0.96 (Fig. 4). The phantom had a length of 700 mm and an outside diameter of 203 mm, and in parallel to the axis of the cylinder, a hole for the line source, with an outside diameter equal to 6.4 mm is drilled through the whole phantom at a radial distance of 45 mm [2, 14]. The line source was inserted in the hole with an outside diameter equal to 3.2 mm and a length of 700 mm (Fig. 4 (A)). In the simulation, the source of back-to-back annihilation photons with an activity of 1 MBq was used. Also, the NEMA norm mentions that for the scatter fraction simulation, the number of acquired prompt coincidences must be at least 500 000. Prompt coincidences are coincidence events acquired in PET such, as true, scattered, and random coincidences [36]. In presented studies, the number of prompt coincidences amounted to 758 000.

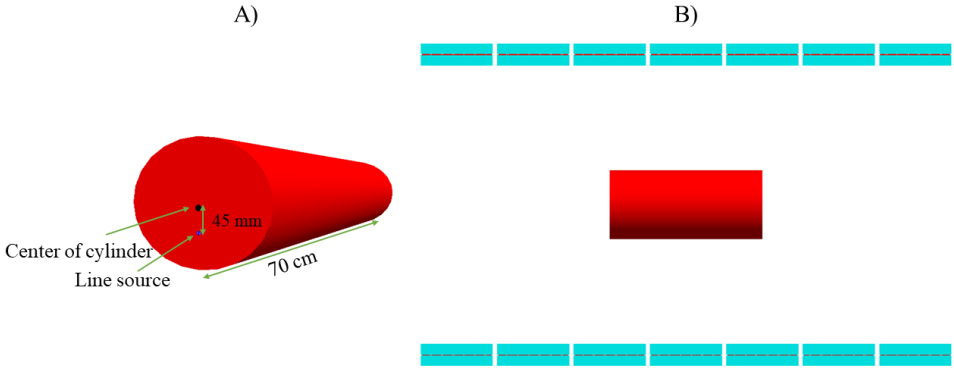

Fig. 4. (A) Schematic view of the simulated phantom model. (B) Top view of the simulated phantom position in the center of the scanner.

3. Result

To extract the true coincidence from all coincidences, the energy larger than the fixed energy threshold (200 keV) was applied. It led to reducing the 88.9% of the scatter and random coincidences. Figure 2 (A) displays the energy distribution for this simulation before applying energy cuts, and Fig. 2 (B) displays the energy distribution after applying the energy cuts. Figure 3 presents the results obtained by using the method based on dividing FOV into 10 mm slices and plotting sinograms for each slice. The Scatter fraction approach was calculated according to NEMA NU 2-2018. Estimated scatter fraction for Total-Body J-PET with the WLS layer is equal to $(45.09 \pm 0.04)\%$ and without the WLS layer is equal to $(44.42 \pm 0.05)\%$. In the presence of WLS, the number of scatter coincidences to total coincidence increases due to introduction of additional material in the scanner.

4. Conclusion

Two models of Total-Body J-PET were simulated to estimate the scatter fraction in the WLS layer according to the NEMA NU 2-2018. Two simulation studies were evaluated with and without the WLS layer inside the detection modules. In this study, the scatter phantom was used with the source of back-to-back annihilation photons with an activity of 1 MBq. Simulations were performed using the GATE with the digitizer simulation toolkit utilized. The analysis process is based on the coincidences part of the digitizer output with the SSRB algorithm. The scatter fraction is expressed as a ratio between the scattered coincidences and the sum of scattered and true coincidences. The final results showed that when Total-Body J-PET has an additional WLS layer, the scatter fraction increases only by around $(0.67 \pm 0.06)\%$. In other words, in the presence of the WLS layer, the ratio of scattering coincidence to total coincidence increases which means that the signal-to-noise ratio is worse. The achieved result for the scatter fraction of the Total-Body J-PET with and without WLS are comparable with the existing tomographs. The scatter fraction for Biograph Vision Quadra with 106 cm AFOV is 36% [21] and for PennPET uExplore with 76.4 cm AFOV is 32% [7].

Authors acknowledge the support of the Foundation for Polish Science through the programme TEAM POIR.04.04.00-00-4204/17; the National Science Centre, Poland (NCN) through grants Nos. 2021/42/A/ST2/00423 and 2021/43/B/ST2/02150; the Ministry of Education and Science under grant No. SPUB/SP/530054/2022; EU Horizon 2020 research and innovation programme, STRONG-2020 project, under grant agreement No. 824093;

the Jagiellonian University via the project CRP/0641.221.2020, and via SciMat and qLife Priority Research Areas under the Strategic Programme Excellence Initiative at the Jagiellonian University.

REFERENCES

[1] A. Alavi *et al.*, *Bio. Algorithms Med. Syst.* **17**, 203 (2021).
[2] P. Kowalski *et al.*, *Phys. Med. Biol.* **63**, 165008 (2018).
[3] S. Vandenberghe *et al.*, *EJNMMI Phys.* **7**, 35 (2020).
[4] P. Moskal *et al.*, *PET Clinics* **15**, 439 (2020).
[5] J. Humm *et al.*, *Eur. J. Nucl. Med. Mol. Imaging* **30**, 1574 (2003).
[6] D. Townsend, *Ann. Acad. Med. Singapure* **33**, 133 (2004).
[7] J. Karp *et al.*, *J. Nucl. Med.* **49**, 462 (2008).
[8] W. Moses *et al.*, *IEEE Trans. Nucl. Sci* **46**, 474 (1999).
[9] W. Moses, *IEEE Trans. Nucl. Sci.* **50**, 1325 (2003).
[10] M. Conti *et al.*, *IEEE Trans. Nucl. Sci.* **56**, 926 (2009).
[11] M. Conti, *Phys. Med.* **25**, 1 (2009).
[12] T. Carlier *et al.*, *EJNMMI Phys.* **7**, 55 (2020).
[13] S. Zein *et al.*, *Med. Phys.* **47**, 1949 (2020).
[14] P. Moskal *et al.*, *Phys. Med. Biol.* **66**, 175015 (2021).
[15] J. Karp *et al.*, *J. Nucl. Med.* **61**, 136 (2020).
[16] A. Pantel *et al.*, *J. Nucl. Med.* **61**, 144 (2020).
[17] V. Viswanath *et al.*, *Phys. Med. Biol.* **65**, 035002 (2020).
[18] B. Spencer *et al.*, *J. Nucl. Med.* **62**, 861 (2021).
[19] R. Badawi *et al.*, *J. Nucl. Med.* **60**, 299 (2019).
[20] R. Badawi *et al.*, *J. Nucl. Med.* **59**, 223 (2018).
[21] G. Prenosil *et al.*, *J. Nucl. Med.* **63**, 476 (2022).
[22] F. Schmidt *et al.*, *J. Nucl. Med.* **61**, 166 (2020).
[23] S. Niedzwiecki *et al.*, *Acta Phys. Pol. B* **48**, 1567 (2017).
[24] P. Moskal *et al.*, *Nucl. Instrum. Methods Phys. Res. A* **764**, 317 (2014).
[25] P. Moskal *et al.*, *Phys. Med. Biol.* **64**, 055017 (2019).
[26] P. Kowalski *et al.*, *Acta Phys. Pol. A* **127**, 1505 (2015).
[27] M. Dadgar *et al.*, *Acta Phys. Pol. B* **51**, 309 (2020).
[28] P. Moskal *et al.*, *Eur. Phys. J. C* **78**, 970 (2018).
[29] P. Moskal *et al.*, *Sci. Adv.* **7**, eabh4394 (2021).
[30] P. Moskal *et al.*, *Nature Commun.* **12**, 5658 (2021).
[31] P. Moskal *et al.*, *Nature Rev. Phys.* **1**, 527 (2019).
[32] P. Moskal *et al.*, *EJNMMI Phys.* **7**, 44 (2020).

[33] P. Moskal *et al.*, *Front. Phys.* **10**, 969806 (2022).

[34] D. Sarrut *et al.*, *Phys. Med. Biol.* **67**, 184001 (2022).

[35] D. Sarrut *et al.*, *Phys. Med. Biol.* **66**, 10TR03 (2021).

[36] NEMA, «Performance Measurements of Positron Emission Tomographs (PET)», NEMA Standards Publication (NEMA NU 2-2018), 2018, https://www.nema.org/standards/view/Performance-Measurements-of-Positron-Emission-Tomographs

[37] J. Smyrski *et al.*, *Nucl. Instrum. Methods Res. Phys. A* **851**, 39 (2017).

[38] J. Smyrski *et al.*, *Bio. Algorithms Med. Syst.* **10**, 59 (2014).

[39] F. Fahey *et al.*, *J. Nucl. Med. Technol.* **30**, 39 (2002).

[40] P. Kowalski *et al.*, *Acta Phys. Pol. B* **47**, 549 (2016).